iScience

CellPress
OPEN ACCESS

Article

A facile spray-pressing synthesis approach for reusable photothermal masks

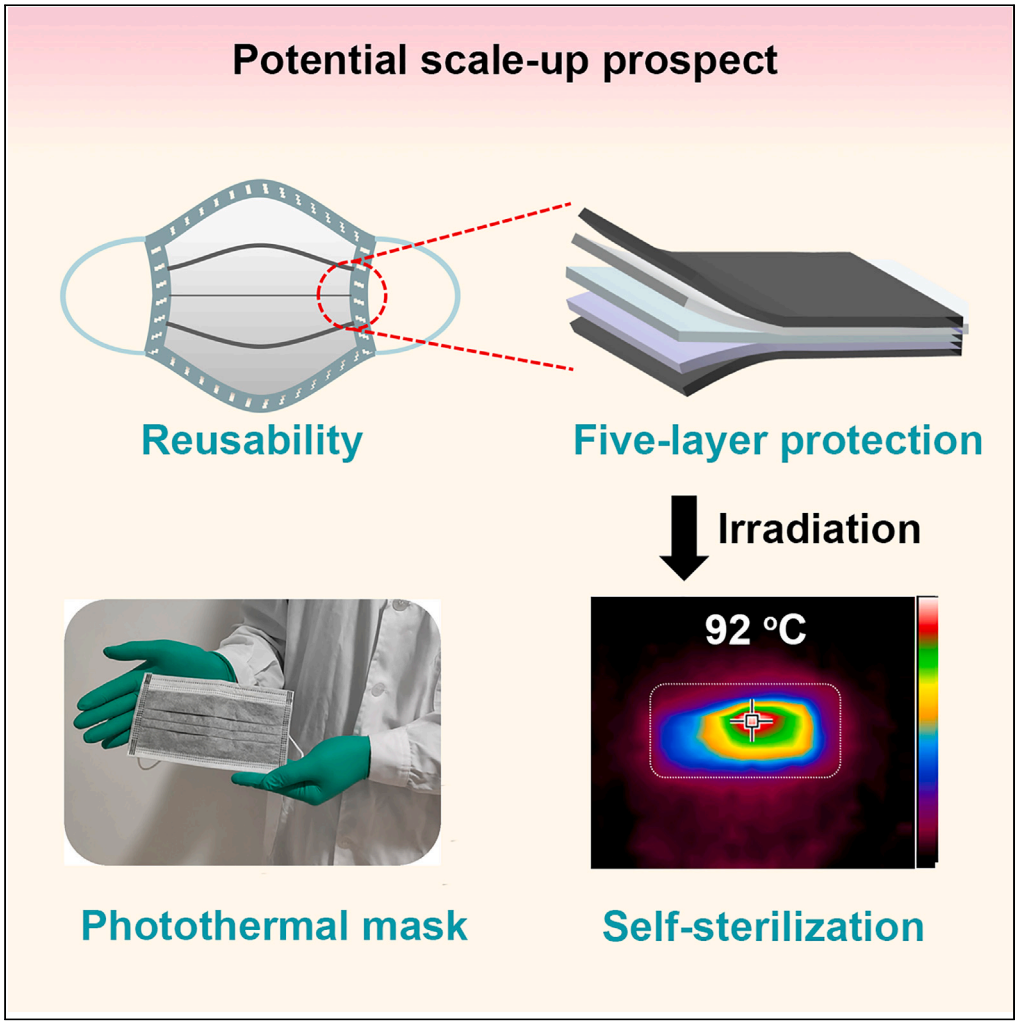

Yi Lu, Yi-Xuan Liu, Yong Wang, ..., Philipp Hügenell, Christoph Janiak, Xiao-Yu Yang

janiak@uni-duesseldorf.de (C.J.)
xyyang@whut.edu.cn (X.-Y.Y.)

Highlights

A facile spray-pressing approach for the production of photothermal mask was present

This technique could be easily integrated into the present automatic mask production

The masks have self-cleaning and/or self-sterilizing properties under irradiation

Lu et al., iScience 26, 107286
August 18, 2023
https://doi.org/10.1016/j.isci.2023.107286

iScience

CellPress
OPEN ACCESS

Article

A facile spray-pressing synthesis approach for reusable photothermal masks

Yi Lu,[1,2,3] Yi-Xuan Liu,[4] Yong Wang,[4] Robert Oestreich,[2] Zi-Yan Xu,[4] Wen Zhang,[4] Philipp Hügenell,[5] Christoph Janiak,[1,2,*] and Xiao-Yu Yang[4,6,*]

SUMMARY

Certain types of face masks are highly efficient in protecting humans from bacterial and viral pathogens, and growing concerns with high safety, low cost, and wide market suitability have accelerated the replacement of reusable face masks with disposable ones during the last decades. However, wearing these masks creates countless problems associated with personnel comfort as well as more significant issues related to the cost of fabrication, the generation of medical waste, and environmental contaminants. In this work, we present a facile spray-pressing technique for the production of P-masks with a potential scale-up prospect by adding a graphene layer on one side of meltblown fabric and a functional layer on the other side. In principle, this technique could be easily integrated into the present automatic mask production process and the masks have self-cleaning and/or self-sterilizing properties when it is exposed to solar or simulated solar irradiation.

INTRODUCTION

Pandemics are human catastrophes and also driving forces of science and technology. This is especially true in the context of medical protection, such as the invention of plague doctors' bird-like masks in the bubonic plague period and the widespread use of face masks during the Manchurian plague 1910 to 1911 and the Spanish flu or Great Influenza pandemic between 1918 and 1920.[1] The rapid development of advanced materials and techniques is the key to fundamental advances in face masks. For example, the meltblown fabric, created by a combination of polymers and nanotechnology, has been chosen as the core layer of disposable masks for virus protection and air permeability.[2] During the last decades, these disposable masks have been the most common form of medical protection equipment due to their high safety and low cost.[3,4] However, many issues have become more obvious after two and a half years of the coronavirus pandemic and need to be addressed properly. For instance, fabrication and disposal of face masks create huge amounts of medical waste, secondary spreading of coronavirus and other environmental pollutants,[5–7] rapid increase of infections in specific regions leads to a shortage of masks,[8] and improper management of discarded masks increases the potential for COVID-19 to spread in medically underserved areas.[9] Reusable masks can greatly mitigate the problems by greatly decreasing mask consumption and stopping the spread of the virus by sterilization.[10,11] Although disposable masks will certainly play a role in the future, their reusable counterparts will become the desired way of protection that avoids the above-mentioned negative effects.[1] Both the researchers and manufacturers should strive to make low-cost, highly protective reusable face masks by finding new advanced materials, up-scaling processes and the use of simple procedures with comprehensive consideration of protection efficiency, comfort, price and environment compatibility to be available against the next possible pandemic attack.

Graphene is a new generation of nanomaterial and possesses excellent photothermal conversion efficiency, outstanding antibacterial and antiviral properties, making it an outstanding sterilization material for reusable masks.[12–14] The graphene-meltblown fabric is the key to the fabrication of reusable masks. There are several aspects to consider: firstly, the graphene layer should be coated uniformly; secondly, any structural damage to the meltblown fabric should be avoided during the synthesis; lastly, any residue of harmful chemical reagents should be avoided. To date, graphene reusable masks can be fabricated using several advanced techniques, such as laser-induced method, ultrasonic extrusion, and coating method.[15–19] However, the limited throughput nature of procedures used for graphene preparation, the expenses of the raw materials and equipment, as well as patent protection issues make this material

[1]Hoffmann Institute of Advanced Materials, Shenzhen Polytechnic, 7098 Liuxian Boulevard, Nanshan District, Shenzhen 518055, China

[2]Institut für Anorganische Chemie und Strukturchemie, Heinrich-Heine-Universität Düsseldorf, Universitätsstraße 1, 40225 Düsseldorf, Germany

[3]School of Chemical Engineering and Technology, Sun Yat-sen University, Zhuhai 519082, China

[4]State Key Laboratory of Advanced Technology for Materials Synthesis and Processing & Shenzhen Research Institute, Wuhan University of Technology, Wuhan 430070, China

[5]Division Thermal Systems and Buildings, Fraunhofer Institute for Solar Energy Systems ISE, Heidenhofstraße 2, Freiburg 79110, Germany

[6]Lead contact

*Correspondence: janiak@uni-duesseldorf.de (C.J.), xyyang@whut.edu.cn (X.-Y.Y.)

https://doi.org/10.1016/j.isci.2023.107286

unsuitable for incorporation into simple face masks at the current time. In this work, we present a facile spray-pressing technique for the production of photothermal masks (P-masks) with a potential scale-up prospect, which is amenable to self-cleaning and/or self-sterilizing protocols that can be executed at the individual level using simple procedures such as exposure to solar or simulated solar irradiation. This approach to mask production could be integrated into the current automated mask manufacturing procedures theoretically, while increasing the cost of the P-mask by only US$0.15 per 100 masks.

By sharing the photothermal mask technique, we hope to increase the diversity of voices concerning the defining ethical considerations of such technologies. Our goal in developing this technique is to make reusable masks available, and give an alternative approach to jointly tackle the issue of global respiratory infectious diseases in the future.

RESULTS AND DISCUSSION

Fabrication technique and characteristics of P-mask

A simple spray-pressing process, as schematically shown in Figure 1A, was developed for depositing graphene onto the surface of the core meltblown polymer layer of commercial masks (C-masks). A graphene ink sprayer is set above the conveyor belt. Each mask is coated with an average of 50 mg of graphene in this process. An optional sprayer can also be installed by adding another coating unit in the same way, if the mask needs to be further functionalized. MIL-160 is one of the most promising metal-organic frameworks (MOFs) for cooling applications due to its water-based synthesis, inexpensive, excellent water vapor adsorption-desorption, and high stability.[20–23] As shown in Figure 1B, the framework with the chemical formula $\{Al(OH)(fum) \cdot nH2O\}_m$ is built up from Al-OH-Al chains connected by fumarate linkers resulting in lozenge-shaped 1D pores. Further, Cadiau et al. firstly synthesized a novel and very promising candidate, which is called MIL-160 (Figure 1C). It consists of helical cis corner-sharing chains of $AlO_4(OH)_2$ octahedra connected by 2,5-furandicarboxylate groups, building one-dimensional square-shaped sinusoidal channels.[24] For example, we coated a MIL-160 layer on the opposite side of the graphene-meltblown to improve the anti-moisture performance by adding another sprayer on the production line.[25,26] Because the current technology for fabricating C-masks is both simple and well-refined, it can be readily modified to incorporate the components needed to carry out the newly designed spaying-pressing process. To understand the interaction of the mask with coating ink, the hydrophobicities of the C-mask and P-mask were measured. As shown in Figure 1D, the meltblown fabric exhibits a water contact angle of 132 $\pm$ 3°, which makes it difficult to achieve uniform coating by the water-ink system due to its high surface tension. In this work, ethanol was used to reduce the surface tension of water. In Figure 1E, the meltblown fabric displays a contact angle of 107 $\pm$ 2° againsts the aqueous ethanol droplet (10%, v/v ethanol), which can ensure that the ink we used can not wet the meltblown fabric. This way avoid damage to the structure of the meltblown fabric during the spray-pressing process. Meanwhile, the reduced contact angle resulted in a favorable contact between graphene/MIL-160 and the meltblown fabric, contributing to the fabrication of functional layers. In our practice, the coating units were manually operated and adjusted, followed by the movement of meltblown fabric (Figure 1F). The meltblown fabric coating with graphene and function layers (MIL-160) has finally been assembled into the "3-layer protection" of P-mask (Figure 1G). Considering the high price of graphene materials, we explored a simple method for the synthesis of graphene. The polymerization process we developed for this purpose has a relatively low cost, and is scalable and safe. The carbon sources for the graphene synthesis process are phthalocyanines or fossil hydrocarbons, such as pitch and high molecular weight aromatic substances.[27] Furthermore, a graphene production plant was built to have an output capacity of 1 ton per year in China, and graphene from this facility has been used in our studies to make P-masks to enable the lower cost of production.

The basic characteristics of the graphene are shown in Figures 1G–1K. The graphene materials in the scanning electron microscope (SEM) image (Figure 1H) show a honeycomb-like structure with the sheets ranging from hundreds of nanometers to a few micrometers. A broad diffraction peak located at around 24.5° in the power X-ray diffraction (XRD) pattern corresponds to the (002) planes of graphene (Figure 1I). The two characteristic peaks located at 1330 cm^{-1} and 1591 cm^{-1} in the Raman spectrum are attributed to the D and G bands (Figure 1J). The broad peak of the 2D band implies that a multilayer of graphene is formed. The thermal stabilities of the P-mask and C-mask were further evaluated by thermogravimetric analysis (TGA) (Figure 1K). The meltblown fabrics obtained from the P-mask and the C-mask showed a rapid decrease of weight in the temperature range from 280°C to 400°C, mainly due to the combustion of polypropylene and graphene in airflow. Considering the instability of polypropylene materials over 130°C,[28] the

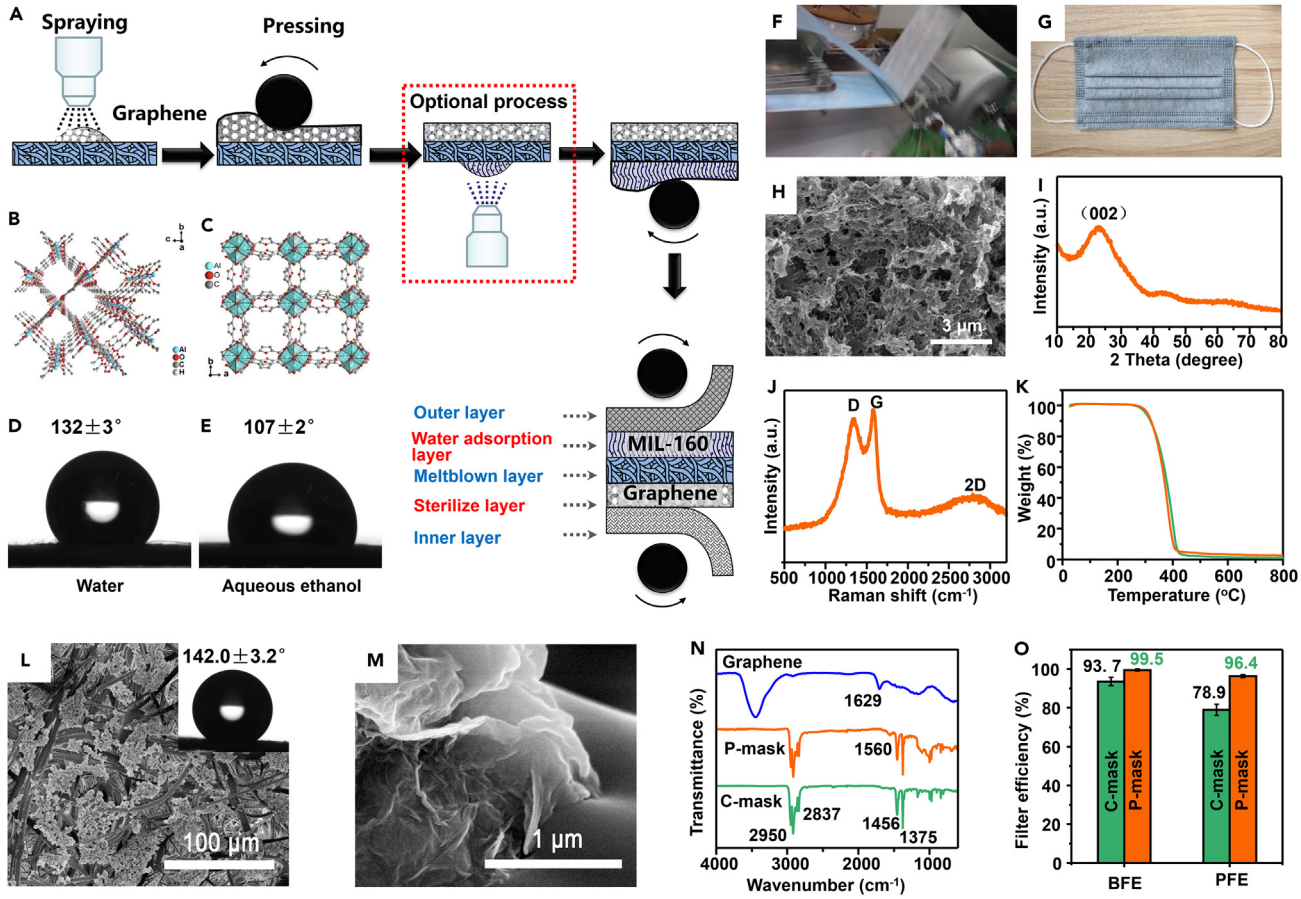

Figure 1. Fabrication and structure of graphene and P-masks

(A) Illustration of the spray-pressing synthesis approach for graphene/MIL-160 coated P-masks.

(B) Crystal structure of aluminum fumarate. Graphic produced by software Diamond from cif-file for Basolite A520 (CCDC no. 1051975). Figure is redrawn from the Supporting Information of ref.[26]

(C) Crystal structure of MIL-160. Graphic produced by software Diamond from cif-file under CCDC no. 1828695.Figure is redrawn from the Supporting Information of ref.[26]

(D) Water and (E) aqueous ethanol droplets deposited on meltblown fabric and their contact angles. (F) End of the spray-pressing production line.

(G) Photograph of an as-prepared P-mask. (H) SEM image of graphene powder.

(I) XRD pattern of graphene.

(J) Raman spectrum of graphene.

(K) TGA analysis of meltblown fabric (green curve) and graphene-meltblown fabric (yellow curve) in airflow.

(L and M) SEM images of the microstructures of the graphene layer, the inset shows the water contact angle on the graphene-meltblown fabric.

(N) FT-IR spectra of the P-mask, C-mask and graphene.

(O) Bacterial filtration efficiency (BFE) and particulate filtration efficiency (PFE) of the P-mask and C-mask, test standard: YY 0469–2011.

photothermal properties lead to a temperature lower than 100°C, controlled by adjusting the thickness of the graphene layer.

The microstructures of the graphene coating surface are observed in Figure 1L. Inspection of these images demonstrate that the nanomaterials are uniformly deposited on meltblown surfaces. This is particularly apparent on the single fabric (Figure 1M). The inset image shows a more hydrophobic surface of the graphene-meltblown fabric than the pristine one, which is attributed to the spiky nanostructures of the hydrophobic graphene layer that increase the surface roughness. The Fourier Transform Infrared Spectroscopy (FT-IR) spectra of meltblown fabric, graphene-meltblown fabric, and graphene are shown in Figure 1N. Graphene exhibits an OH peak at 3445 cm^{-1}, a C=C peak at 1629 $cm^{-1}$and weak signals from C-O functionalities such as COC/COH (1376-1064 cm^{-1}). The green curve represents the typical polypropylene feature. The peaks around 1456 and 1375 cm^{-1} are assigned to -CH_2- bending vibrations of methylene

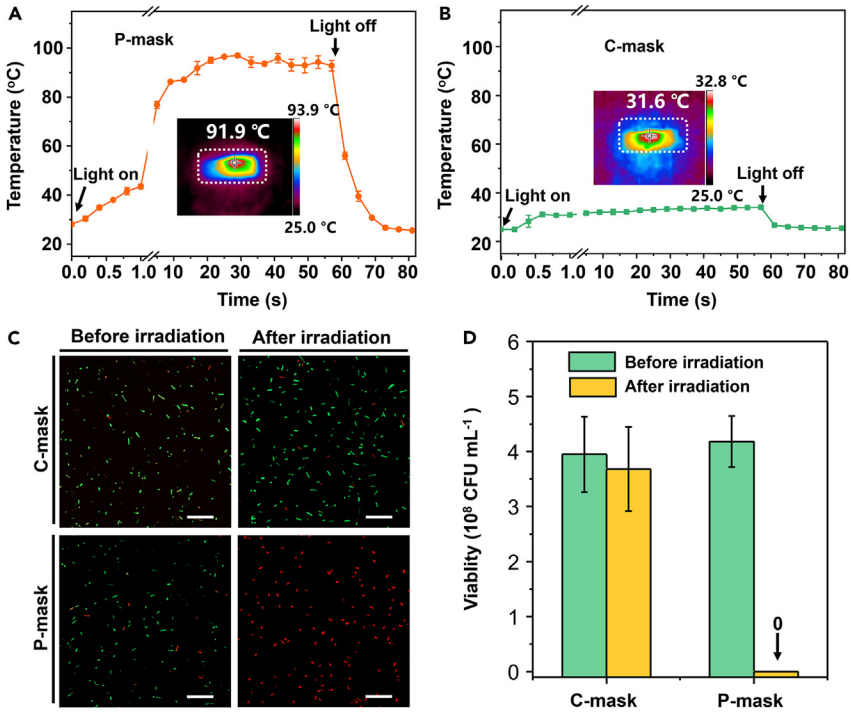

Figure 2. Photothermal antibacterial ability tests

(A and B) Surface temperatures of (A) P-mask and (B) C-mask in response to simulated solar irradiation (200 mW cm^2), insets are photographs of masks after 30 s of illumination.

(C) Laser scanning confocal microscopy images of *E. coli* ATCC 25922 on the P-mask and C-mask after treatment with SYTO 9 and propidium iodide (scale bar = 10 μm).

(D) The number of viable E. coli, calculated from the CFU count, after solar irradiation treatment with the P-mask and C-mask.

groups and -CH_3 bending vibrations of methyl groups, respectively.[29] The peaks due to the -CH_3 stretching vibration overlap with the -CH_2- stretching vibration and can be seen ranging from 2837 to 2949 cm^{-1}.[30] Numerous small peaks in the wavenumber range 1167-808 cm^{-1} are assigned to C-C stretching vibrations, CH_3 asymmetric rocking, C-H wagging vibrations and CH_2 rocking vibrations.[31] After coating with graphene, a new peak that appeared at 1560 cm^{-1} is attributed to the stretching bands of N-H from the amide, implying the interaction between the meltblown fabric and graphene via a coupling reaction.[32] There is also a small C=C peak at 1621 cm^{-1} corresponding to the sp^2 character of graphene. The bacterial filtration efficiency (BFE) and particulate filtration efficiency (PFE) of both the P-mask and C-masks were evaluated using procedures suggested by the Technical Standard of Surgical Masks (YY 0469–2011). The results in Figure 1O show that the P-masks have a BFE of 99.5% and a PFE of 96.4%, both of which are superior to those of N95 masks. In contrast, the C-masks have a BFE value of 93.7% and a PFE of 78.9%, indicating that the coating treatment can greatly improve the filtration efficiency of the mask.

Analysis of the photothermal antibacterial properties

The photothermal antibacterial ability has been examined. The temperature of the graphene-meltblown fabric rapidly responds to simulated solar irradiation. As shown in Figure 2A, simulated solar irradiation causes the temperature of the surface of the P-mask to change from room temperature to 43°C within 1 s, to over 76°C within 4 s, and then to a plateau around 93–97°C. The level of temperature increase is sufficient to simultaneously dry the mask and kill or inactivate viruses without causing damage to the meltblown fabric.[33] Owing to the high photothermal conversion efficiency of the graphene layer, the temperature of the mask can increase to *ca.* 65°C when it is exposed to direct outdoor solar irradiation if we extend the exposure time. It should be noted that the outdoor solar intensity relies on longitude/latitude, weather, season, sunlight incidence angle, et al., therefore direct outdoor solar irradiation is hard to be a standard to evaluate the photothermal antibacterial ability. In contrast, the C-mask undergoes only a slight temperature change (Figure 2B) under simulated solar sunlight irradiation.

We further investigated the photothermal antibacterial abilities and the *E. coli* ATCC 25922 strain was used due to its matching thermotolerance to the test.[34,35] During the test, a 100 μL aliquot of bacterial suspension was dropped onto each mask, forming a droplet retained on the surface of mask due to the hydrophobicity of the meltblown fabric (see Figure S1). When the sample was treated with solar irradiation, the temperature of the graphene layer increased very quickly and heated the droplet to a high temperature. The thermal camera shows the temperature reached up to 96°C under irradiation. And the temperature of the surface dropped from 96°C to 62°C–74°C and stabilized above 60°C when the light was turned off (see Video S1). Considering the heat loss after turning off the light, we think the temperature of the droplet was much higher than the displayed temperature. In real conditions, viruses are directly adsorbed on the surface of the P-mask, the sterilization temperature is up to 90°C under the simulated solar irradiation and the photothermal antibacterial efficiency should be much higher than our experiment. And the photothermal antibacterial ability is designed for available under 2-sun irradiation is considered from a safety point of view. For example, if the temperature of the mask can increase to 90°C under real sunlight irradiation, it's not safe for wearing and storage.

The *E. coli* bacteria were then collected and cultured on an LB agar plate for 24 h. The condition of bacterial culture growth on the P-mask and C-mask was observed by laser scanning confocal microscopy. As shown in Figure 2C, the red dots replaced the green dots in the photograph after the P-mask had been irradiated, indicating that all *E. coli* on the P-mask were dead. This is mainly attributed to the photothermal antibacterial properties of the P-mask under solar irradiation. On the contrary, the *E. coli* on the C-mask were all still alive after light irradiation. Figure 2D displays the statistics of colony-forming units (CFUs) in two samples. Over 93% of the *E. coli* deposited on the C-mask remained alive after irradiation for 10 min, indicating the negligible photothermal antibacterial effects of the C-mask. In comparison, the viability of *E. coli* on the P-mask dropped from 4.2×10^8 to almost 0 CFU mL^{-1} after irradiation, which was consistent with fluorescence-based live/dead assay. The photothermal effect of the graphene layer remarkably contributes to the self-sterilization of the mask by lethally affecting the proteins and nucleic acids of bacteria, which is the main mechanism of its extensive antibacterial activity.

Analysis of the reusability properties of P-mask

To improve the stability of functional layers on the surface of meltblown fabric, 3-aminopropyltriethoxysilane (APTES) was used. The APTES could be hydrolyzed during the ink preparation. These hydrolysis products can be co-deposited on the meltblown fabric surfaces with graphene/MIL-160 via hydrogen bonding and physical entanglement, which may endow the graphene/MIL-160 layer with special stability.[36–38] To assess whether our P-masks will be effective under real-time conditions, we have measured the durability of the multi-layer structure and sterilization properties. The P-masks were first exposed to steam at 100°C for 30 min. After drying, the P-mask was ventilated with N_2 flow to simulate human exhalation for 60 min and folded 200 times by hand, and then it was irradiated for 1 h. As shown in Figure 3A, no nanoparticles or graphene sheets are found on the inner layer of the P-mask in SEM images after N_2 purging. Even after 200 times of folding, no graphene "drop" from the meltblown fabric to the inner layer was observed (Figure 3B), suggesting that the nanoparticles are firmly coated on the meltblown fabric.

Next, we dropped the *E. coli* solution on the treated masks to investigate the antibacterial activities. From Figure 3C, we can see that nearly all of the bacteria loaded onto the masks maintained viability on the fluorescence microscopy photograph. After the photothermal antibacterial process, only dead bacteria were observed under fluorescent microscopy and no surviving bacteria were found for plate incubation. We also calculated the CFUs on the plates by counting the surviving bacteria in Figure 3D. There were about 3.4×10^8 CFU mL^{-1} on the treated P-mask before irradiation, which is close to that of the pristine P-mask. After light irradiation, we did not find any bacterial colony in the LB agar plate, suggesting that the treated P-mask has exercised a high photothermal antibacterial property.

Then the P-mask was checked by FT-IR to evaluate its structural stability. As shown in Figure 3E, the main vibration peaks of the treated P-mask are the same as those of the pristine P-mask (see Figure 1J), indicating that the molecular structure of the graphene-meltblown was not altered by the treatment or the temperature. The long-term anti-moisture properties were experimentally determined. The water sorption properties of the MIL-160 part of the P-masks were determined by using a humidified argon flow and an alternating temperature regime to simulate human breath. For this purpose, the MIL-160 coating was measured under humidified argon using a microbalance over 50 repeated cycles of rapid temperature

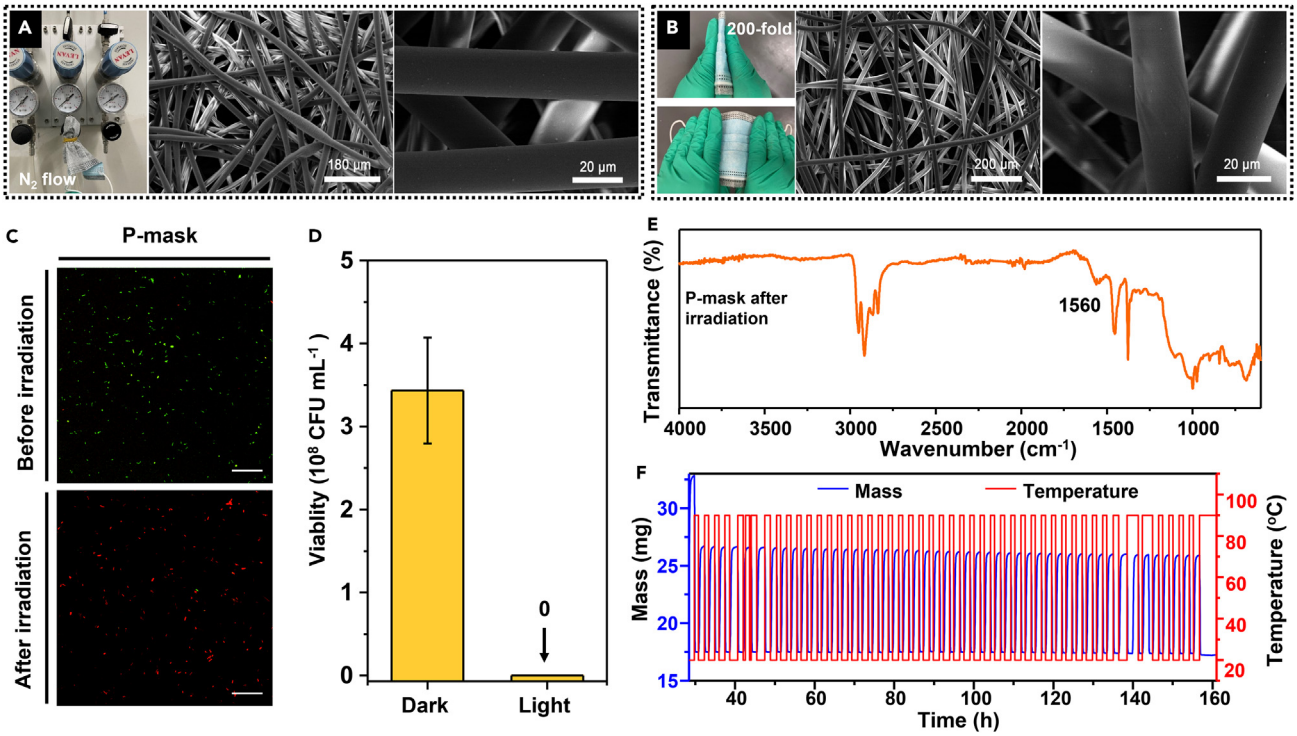

Figure 3. Photothermal reusability of the P-mask

(A) Photograph of ventilating the P-mask with N_2 flow to simulate human exhalation and SEM images of the inner layer after 60 min of ventilation.

(B) Photograph of a folding-unfolding experiment of the P-mask and SEM images of the inner layer after 200 times of folding.

(C) Laser scanning confocal microscopy images of E. coli on the P-mask after steam treatment, folding experiment, before and after 60 min of irradiation treatment.

(D) Number of viable *E. coli* on the P-mask after steam treatment, folding experiment, before and after 60 min of irradiation treatment.

(E) FT-IR spectrum of the P-mask after irradiation treatment.

(F) Mass and temperature changes associated with water sorption of MIL-160 from a humidified argon flow over 50 cycles of reversible temperature changes from 20°C (adsorption) and 90°C (desorption).

changes between 20°C (water adsorption) and 90°C (water desorption). The results (Figure 3F) show that the amount of water adsorbed during each cycle slowly and slightly decreases until it reaches a minimal level. Analysis of the data shows that the total weight of water uptake versus the weight of the coating material is ca. 0.53 g/g during initial cycles and ca. 0.49 g/g at the 50th cycle. Thus, no significant change occurs in the total water uptake capacity during the 50-cycle process. Importantly, the as-prepared mask containing a nanoscale functional graphene layer, has a high air permeability and displays a rapid temperature response to solar irradiation (Figures 2A and 2B). Besides, our graphene has a cost of US$30 per kilogram, which is much lower than that associated with other currently utilized methods and increases the cost of the P-mask by only US$0.15 per 100 masks. As a result, the P-masks can adsorb the incoming and possible virus-loaded water droplets arising from human breath and desorb water while killing viruses under solar or simulated solar irradiation, which mask the P-masks highly affordable and reusable.

Expansion of our technique in common fabrics

In earlier studies of the filtration properties of common household materials, it was found that cotton and polypropylene multilayered structures meet or even exceed the filtration efficiencies of meltblown fabrics.[39] It will be interesting to determine if the graphene and function layers can be applied to common household materials. We performed additional experiments to explore the consequences of coating household materials such as linen, cotton, gauze, and silk with graphene by using the simple spray-pressing process. Microstructures of these coating surfaces in SEM are more ordered and have larger diameters (Figures 4A–4D). Inspection of optical images shows that graphene is uniformly coated on the surfaces of these fabrics. The findings show that household materials can be used as the basis for wonderful reusable masks by using our technique during the pandemic.

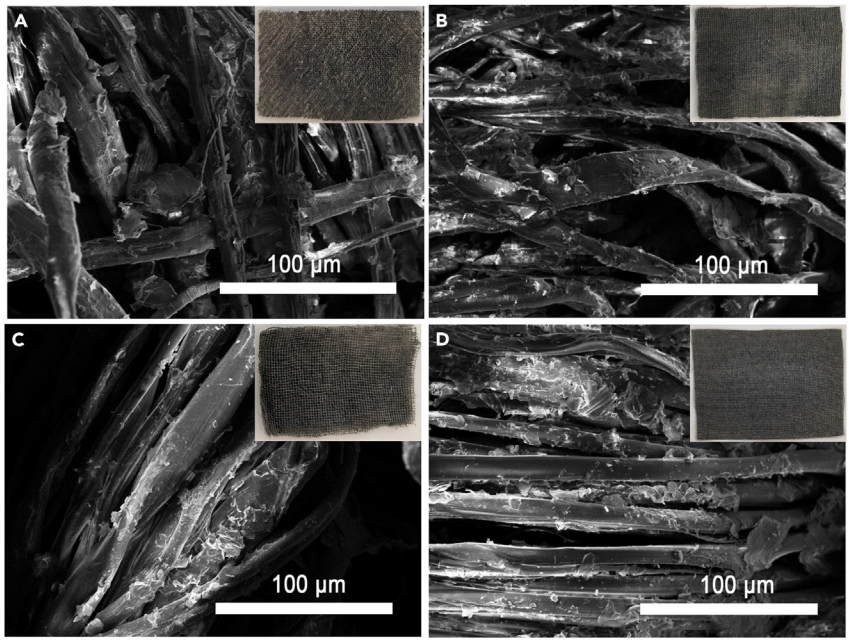

Figure 4. The morphology of different filtration materials

(A–D) SEM images of the microstructures of graphene on linen, cotton, gauze and silk, respectively, deposited using the developed spray-pressing process (the insets are corresponding optical images).

Reflecting on the pandemic, it is clear that while the public health crisis was global during the last three years, the responses to date have been devised mostly in individual countries, and some international co-operations in research and organization (such as World Health Organization). In this technical report, we introduced a P-mask technique, which can be self-cleaned and/or self-sterilized by solar or simulated solar irradiation. Our goal was to decrease the damage caused by the pandemic and afford the urgent demand for safe reusable masks in the further. An approach involving the use of effective and reusable face masks could represent a global solution to combating respiratory infectious diseases in the future, particularly those that occur in undeveloped areas.

Limitations of the study

In this work, the graphene layer has great effects on temperature during irradiation, including the coating thickness and consistency of the graphene. We controlled the temperature by adjusting the weight of graphene sheets per mask, but a precise relationship between the temperature of the P-mask and the thickness of the graphene layer cannot be obtained. To detail the experiment, this relationship data needs to be provided by more studies in further research.

STAR★METHODS

Detailed methods are provided in the online version of this paper and include the following:

- KEY RESOURCES TABLE
- RESOURCE AVAILABILITY
  - Lead contact
  - Materials availability
  - Data and code availability
- EXPERIMENTAL MODEL AND SUBJECT DETAIL
  - Method details
  - Quantification and statistical analysis

SUPPLEMENTAL INFORMATION

Supplemental information can be found online at https://doi.org/10.1016/j.isci.2023.107286.

ACKNOWLEDGMENTS

This study was supported by the Sino-German Centre's COVID-19 Related Bilateral Collaborative project (C-0046), joint NSFC-DFG Project (NSFC grant 51861135313, DFG JA466/39-1), National 111 project (B20002), Program for Changjiang Scholars and Innovative Research Team in University (IRT_15R52), Guangdong Basic and Applied Basic Research Foundation (2022A1515010137), Shenzhen Science and Technology Program (GJHZ20210705143204014, JCYJ20210324142010029, KCXFZ20211020170006010).

AUTHOR CONTRIBUTIONS

Conceptualization, Y.L., X.Y.Y.; Methodology, Y.L.; Investigation, Y.X.L, Y.W., R.O., Z.Y.X., W.Z., P.H.; Writing - Original Draft, Y.L.; Writing – Review & Editing, Y.L., R.O., X.Y.Y. and C.J.; Funding Acquisition, X.Y.Y. and C.J.; Resources, X.Y.Y. and C.J.; Supervision, X.Y.Y. and C.J.

DECLARATION OF INTERESTS

The authors declare that they have no known competing financial interests or personal relationships that could have appeared to influence the work reported in this paper.

INCLUSION AND DIVERSITY

We support inclusive, diverse, and equitable conduct of research.

Received: October 19, 2022
Revised: June 26, 2023
Accepted: June 30, 2023
Published: July 11, 2023

REFERENCES

1. Strasser, B.J., and Schlich, T. (2020). A history of the medical mask and the rise of throwaway culture. Lancet *396*, 19–20. https://doi.org/10.1016/S0140-6736(20)31207-1.

2. Spooner, J.L. (1967). History of Surgical Face Masks. AORN J. *5*, 76–80. https://doi.org/10.1016/S0001-2092(08)71359-0.

3. Johnson, D.F., Druce, J.D., Birch, C., and Grayson, M.L. (2009). A Quantitative Assessment of the Efficacy of Surgical and N95 Masks to Filter Influenza Virus in Patients with Acute Influenza Infection. Clin. Infect. Dis. *49*, 275–277. https://doi.org/10.1086/600041.

4. Leung, N.H.L., Chu, D.K.W., Shiu, E.Y.C., Chan, K.-H., McDevitt, J.J., Hau, B.J.P., Yen, H.-L., Li, Y., Ip, D.K.M., Peiris, J.S.M., et al. (2020). Respiratory virus shedding in exhaled breath and efficacy of face masks. Nat. Med. *26*, 676–680. https://doi.org/10.1038/s41591-020-0843-2.

5. Patrício Silva, A.L., Prata, J.C., Walker, T.R., Duarte, A.C., Ouyang, W., Barcelò, D., and Rocha-Santos, T. (2021). Increased plastic pollution due to COVID-19 pandemic: Challenges and recommendations. Chem. Eng. J. *405*, 126683. https://doi.org/10.1016/j.cej.2020.126683.

6. Li, B., Huang, Y., Guo, D., Liu, Y., Liu, Z., Han, J.-C., Zhao, J., Zhu, X., Huang, Y., Wang, Z., and Xing, B. (2022). Environmental risks of disposable face masks during the pandemic of COVID-19: Challenges and management. Sci. Total Environ. *825*, 153880. https://doi.org/10.1016/j.scitotenv.2022.153880.

7. Bondaroff, T.P., and Cooke, S. (2020). Masks on the Beach: The Impact of COVID-19 on Marine Plastic Pollution.

8. Hantoko, D., Li, X., Pariatamby, A., Yoshikawa, K., Horttanainen, M., and Yan, M. (2021). Challenges and practices on waste management and disposal during COVID-19 pandemic. J. Environ. Manag. *286*, 112140. https://doi.org/10.1016/j.jenvman.2021.112140.

9. Nzediegwu, C., and Chang, S.X. (2020). Improper solid waste management increases potential for COVID-19 spread in developing countries. Resour. Conserv. Recycl. *161*, 104947. https://doi.org/10.1016/j.resconrec.2020.104947.

10. Zakrzewska, A., Haghighat Bayan, M.A., Nakielski, P., Petronella, F., De Sio, L., and Pierini, F. (2022). Nanotechnology Transition Roadmap toward Multifunctional Stimuli-Responsive Face Masks. ACS Appl. Mater. Interfaces *14*, 46123–46144. https://doi.org/10.1021/acsami.2c10335.

11. De Sio, L., Ding, B., Focsan, M., Kogermann, K., Pascoal-Faria, P., Petronela, F., Mitchell, G., Zussman, E., and Pierini, F. (2021). Personalized Reusable Face Masks with Smart Nano-Assisted Destruction of Pathogens for COVID-19: A Visionary Road. Chem. Eur. J. *27*, 6112–6130. https://doi.org/10.1002/chem.202004875.

12. Li, Z., Lei, H., Kan, A., Xie, H., and Yu, W. (2021). Photothermal applications based on graphene and its derivatives: A state-of-the-art review. Energy *216*, 119262. https://doi.org/10.1016/j.energy.2020.119262.

13. Maqbool, I., Rehman, F., Soomro, F., Bhatti, Z., Ali, U., Jatoi, A.H., Lal, B., Iqbal, M., Phulpoto, S., Ali, A., and Thebo, K.H. (2021). Graphene-based Materials for Fighting Coronavirus Disease 2019: Challenges and Opportunities. ChemBioEng Rev. *8*, 67–77. https://doi.org/10.1002/cben.202000039.

14. Deng, W., Sun, Y., Yao, X., Subramanian, K., Ling, C., Wang, H., Chopra, S.S., Xu, B.B., Wang, J.-X., Chen, J.-F., et al. (2022). Masks for COVID-19. Adv. Sci. *9*, 2102189. https://doi.org/10.1002/advs.202102189.

15. Huang, L., Xu, S., Wang, Z., Xue, K., Su, J., Song, Y., Chen, S., Zhu, C., Tang, B.Z., and Ye, R. (2020). Self-Reporting and Photothermally Enhanced Rapid Bacterial Killing on a Laser-Induced Graphene Mask. ACS Nano *14*, 12045–12053. https://doi.org/10.1021/acsnano.0c05330.

16. Lin, Z., Wang, Z., Zhang, X., and Diao, D. (2021). Superhydrophobic, photo-sterilize, and reusable mask based on graphene nanosheet-embedded carbon (GNEC) film. Nano Res. *14*, 1110–1115. https://doi.org/10.1007/s12274-020-3158-1.

17. Zhong, H., Zhu, Z., Lin, J., Cheung, C.F., Lu, V.L., Yan, F., Chan, C.-Y., and Li, G. (2020). Reusable and Recyclable Graphene Masks with Outstanding Superhydrophobic and Photothermal Performances. ACS Nano *14*, 6213–6221. https://doi.org/10.1021/acsnano.0c02250.

18. De Maio, F., Palmieri, V., Babini, G., Augello, A., Palucci, I., Perini, G., Salustri, A., Spilman, P., De Spirito, M., Sanguinetti, M., et al. (2021). Graphene nanoplatelet and graphene oxide functionalization of face mask materials inhibits infectivity of trapped SARS-CoV-2. iScience *24*, 102788. https://doi.org/10.1016/j.isci.2021.102788.

19. Seidi, F., Deng, C., Zhong, Y., Liu, Y., Huang, Y., Li, C., and Xiao, H. (2021). Functionalized Masks: Powerful Materials against COVID-19 and Future Pandemics. Small *17*, 2102453. https://doi.org/10.1002/smll.202102453.

20. Steinert, D.M., Schmitz, A., Fetzer, M., Seiffert, P., and Janiak, C. (2022). A caveat on the effect of modulators in the synthesis of the aluminum furandicarboxylate metal-organic framework MIL-160. Z. Anorg. Allg. Chem. *648*, e202100380. https://doi.org/10.1002/zaac.202100380.

21. Schlüsener, C., Jordan, D.N., Xhinovci, M., Matemb Ma Ntep, T.J., Schmitz, A., Giesen, B., and Janiak, C. (2020). Probing the limits of linker substitution in aluminum MOFs through water vapor sorption studies: mixed-MOFs instead of mixed-linker CAU-23 and MIL-160 materials. Dalton Trans. *49*, 7373–7383. https://doi.org/10.1039/D0DT01044H.

22. Tannert, N., Jansen, C., Nießing, S., and Janiak, C. (2019). Robust synthesis routes and porosity of the Al-based metal–organic frameworks Al-fumarate, CAU-10-H and MIL-160. Dalton Trans. *48*, 2967–2976. https://doi.org/10.1039/C8DT04688C.

23. Permyakova, A., Skrylnyk, O., Courbon, E., Affram, M., Wang, S., Lee, U.-H., Valekar, A.H., Nouar, F., Mouchaham, G., Devic, T., et al. (2017). Synthesis Optimization, Shaping, and Heat Reallocation Evaluation of the Hydrophilic Metal–Organic Framework MIL-160(Al). ChemSusChem *10*, 1419–1426. https://doi.org/10.1002/cssc.201700164.

24. Cadiau, A., Lee, J.S., Damasceno Borges, D., Fabry, P., Devic, T., Wharmby, M.T., Martineau, C., Foucher, D., Taulelle, F., Jun, C.-H., et al. (2015). Design of Hydrophilic Metal Organic Framework Water Adsorbents for Heat Reallocation. Adv. Mater. *27*, 4775–4780. https://doi.org/10.1002/adma.201502418.

25. Schlüsener, C., Xhinovci, M., Ernst, S.-J., Schmitz, A., Tannert, N., and Janiak, C. (2019). Solid-Solution Mixed-Linker Synthesis of Isoreticular Al-Based MOFs for an Easy Hydrophilicity Tuning in Water-Sorption Heat Transformations. Chem. Mater. *31*, 4051–4062. https://doi.org/10.1021/acs.chemmater.9b00617.

26. Gökpinar, S., Ernst, S.-J., Hastürk, E., Möllers, M., El Aita, I., Wiedey, R., Tannert, N., Nießing, S., Abdpour, S., Schmitz, A., et al. (2019). Air-Con Metal–Organic Frameworks in Binder Composites for Water Adsorption Heat Transformation Systems. Ind. Eng. Chem. Res. *58*, 21493–21503. https://doi.org/10.1021/acs.iecr.9b04394.

27. Feng, C., Lu, Y., Liu, Y., Yang, X., and Tian, G. (2022). A facile synthesis of hierarchically porous graphene for high-performance lithium storage. New J. Chem. *46*, 9999–10003. https://doi.org/10.1039/D2NJ02047E.

28. Liao, L., Xiao, W., Zhao, M., Yu, X., Wang, H., Wang, Q., Chu, S., and Cui, Y. (2020). Can N95 Respirators Be Reused after Disinfection? How Many Times? ACS Nano *14*, 6348–6356. https://doi.org/10.1021/acsnano.0c03597.

29. Ko, W.C., and Bresee, R.R. (2003). FT-IR Microspectroscopic Study of Shot Formation in Melt-Blown Webs. Appl. Spectrosc. *57*, 636–641.

30. Senthil Kumar, P., Palaniyappan, M., Priyadharshini, M., Vignesh, A.M., Thanjiappan, A., Sebastina Anne Fernando, P., Tanvir Ahmed, R., and Srinath, R. (2014). Adsorption of basic dye onto raw and surface-modified agricultural waste. Environ. Prog. Sustain. *33*, 87–98. https://doi.org/10.1002/ep.11756.

31. Socrates, G. (2001). Infrared and Raman Characteristic Group Frequencies: Tables and charts, 3rd Edition (John Wiley & Sons).

32. Ou, J., Wang, J., Liu, S., Mu, B., Ren, J., Wang, H., and Yang, S. (2010). Tribology Study of Reduced Graphene Oxide Sheets on Silicon Substrate Synthesized via Covalent Assembly. Langmuir *26*, 15830–15836. https://doi.org/10.1021/la102862d.

33. Yang, P., and Wang, X. (2020). COVID-19: a new challenge for human beings. Cell. Mol. Immunol. *17*, 555–557. https://doi.org/10.1038/s41423-020-0407-x.

34. Li, Q., Yin, Y., Cao, D., Wang, Y., Luan, P., Sun, X., Liang, W., and Zhu, H. (2021). Photocatalytic Rejuvenation Enabled Self-Sanitizing, Reusable, and Biodegradable Masks against COVID-19. ACS Nano *15*, 11992–12005. https://doi.org/10.1021/acsnano.1c03249.

35. Kumar, S., Karmacharya, M., Joshi, S.R., Gulenko, O., Park, J., Kim, G.-H., and Cho, Y.-K. (2021). Photoactive Antiviral Face Mask with Self-Sterilization and Reusability. Nano Lett. *21*, 337–343. https://doi.org/10.1021/acs.nanolett.0c03725.

36. Wu, R., Song, M., Sui, D., Duan, S., and Xu, F.-J. (2022). A natural polysaccharide-based antibacterial functionalization strategy for liquid and air filtration membranes. J. Mater. Chem. B *10*, 2471–2480. https://doi.org/10.1039/D1TB02273C.

37. Cao, S., Ge, W., Yang, Y., Huang, Q., and Wang, X. (2022). High strength, flexible, and conductive graphene/polypropylene fiber paper fabricated via papermaking process. Adv. Compos. Hybrid Mater. *5*, 104–112. https://doi.org/10.1007/s42114-021-00374-2.

38. Nueraji, M., Toktarbay, Z., Ardakkyzy, A., Sridhar, D., Algadi, H., Xu, B.B., Althakafy, J.T., Alanazi, A.K., Abo-Dief, H.M., Adilov, S., and Guo, Z. (2023). Mechanically-robust electrospun nanocomposite fiber membranes for oil and water separation. Environ. Res. *220*, 115212. https://doi.org/10.1016/j.envres.2023.115212.

39. Konda, A., Prakash, A., Moss, G.A., Schmoldt, M., Grant, G.D., and Guha, S. (2020). Aerosol Filtration Efficiency of Common Fabrics Used in Respiratory Cloth Masks. ACS Nano *14*, 6339–6347. https://doi.org/10.1021/acsnano.0c03252.

STAR★METHODS

KEY RESOURCES TABLE

REAGENT or RESOURCE	SOURCE	IDENTIFIER
Bacterial and virus strains		
E. coli	ATCC	25922
Chemicals, peptides, and recombinant proteins		
Premixed PBS Buffer	Aladdin	Cat#P397924-5EA
Ethanol absolute	Sinopharm	CAS: 64-17-5
(3-Aminopropyl)triethoxysilane	Aladdin	CAS: 919-30-2
SYTO 9	Maokangbio	Cat#MX4229-20UL
Propidium iodide	Sigma-Aldrich	CAS: 25535-16-4
Meltblown fabric	Alibaba	N/A
Graphene	Qingdao	N/A

RESOURCE AVAILABILITY

Lead contact

Further information and requests for resources and reagents should be directed to and will be fulfilled by the lead contact, Xiao-Yu Yang, (xyyang@whut.edu.cn).

Materials availability

This study did not generate new unique reagents.

Data and code availability

- Data reported in this paper will be shared by the lead contact upon request.
- This paper does not report original code.
- Any additional information required to reanalyze the data reported in this paper is available from the lead contact upon request

EXPERIMENTAL MODEL AND SUBJECT DETAIL

E. coli ATCC 25922 from stock was streaked onto a Luria-Bertani (LB) agar plate and incubated at 37°C. The isolated colony that appeared after 24 h of incubation was inoculated in 250 mL of LB liquid medium and incubated at 37°C until the logarithmic phase was achieved.

Method details

Synthesis of MIL-160

The framework with the chemical formula {Al(OH)(fum) • nH_2O}m is built up from Al-OH-Al chains connected by fumarate linkers resulting in lozenge-shaped 1D pores. Further, a novel and very promising candidate is MIL-160. It consists of helical cis corner-sharing chains of $AlO_4(OH)_2$ octahedra connected by 2,5-furandicarboxylate groups, building one-dimensional square-shaped sinusoidal channels. The synthesis and more structure details of MIL-160 please see our previously reported studies. MIL-160 was synthesized following the procedure[23]: $Al(OH)(CH_3COO)_2$(37.5 mmol) and 2,5-furandicarboxylic acid (37.5 mmol) were added to a round-bottomed flask (250 mL) containing distilled water (37.5 mL). Followed by stirring under reflux for 24 h, the resulting white solid was recovered by filtration, washed with ethanol, and dried in the oven at 100° C.

Preparation of graphene and MIL-160 inks

Graphene powder (5 g) was dispersed in 1000 mL of a 10% (v/v) aqueous ethanol solution with ultrasonication for at least 60 min. Followed by adding 5 mL of (3-aminopropyl)triethoxysilane, the mixture was stirred for 30 min at room temperature. The MIL-160 ink was prepared by dispersing 10 g of MIL-160 powder in 1000 mL of 10% (v/v) aqueous ethanol solution. Followed by adding 1 mL of (3-aminopropyl)triethoxysilane, the resulting solution was stirred for 30 min.

The P-mask and C-masks were fabricated by using the same type of meltblown fabrics on the nonwoven face mask-making machine production line in Hubei province, China. 10 mL of the above inks are sprayed on the meltblown fabric for each mask.

Fabrication process

The designed coating unit is comprised of a sprayer with a volume of 1200 mL and set over the conveyor belt on a Face Mask Maker Machine (KF94). Before starting the fabrication, the sprayers were filled with graphene and MIL-160 ink. The modified automated system includes components needed to carry out the sequence of steps, including raw material feeding and inserting, coating, drying, and nose wire insertion and sealing, to prepare the finished mask. As the conveyor belt moves forward, graphene ink is sprayed onto the meltblown layer under 0.2 MPa air flow, then pressed by the incorporated wheel and finally assembled into masks.

Characterization

Thermogravimetry analyses (TGA, NETZSCH STA 2500) were performed in the range of 30°C–800°C at a heating rate of 10 °C min^{-1}. The sample morphology was imaged on an SEM (S-4800, HITACHI). The powder X-ray diffraction (XRD) patterns were obtained on a Bruker D8 Advance diffractometer with Cu Kα radiation. Fourier transform infrared spectroscopy (FT-IR) spectra were measured on a Nicolet 6700 (Thermo Scientific) with an attenuated total reflectance method. Raman analysis was performed using a Renishaw InVia Raman spectrometer under visible excitation at 633 nm. The filtration efficiency of masks was assessed on a bacterial filtration efficiency tester (ZR-1000) with gas flowmeter: 28.3 L/min, test Strain: Staphylococcus aureus ATCC 6538, positive quality control value: 2100 CFU, and particle filter efficiency tester (ZR-1006) with 0.3 μm NaCl aerosol and gas flowmeter: 32 L/min. Water sorption isotherms were collected on a vapor sorption analyzer (VSTAR) from Quantachrome. The tubes including the samples were degassed under vacuum at 100°C for 3 h. The samples were attached to the analysis port and measurements were started. A PLS-SXE300D Xenon lamp source was used for the evaporation tests with a light intensity of 200 mW cm^{-2}. Live/dead cell viability assays were performed on a laser scanning confocal microscopy (LSM 980 Zeiss).

Analysis of the photothermal antibacterial ability

The photothermal antibacterial ability of the masks was determined using the *E. coli* ATCC 25922 strain and streaked onto a Luria-Bertani (LB) agar plate and incubated at 37°C. After incubation, the isolated colony was inoculated and incubated to use. In a typical procedure, 100 μL of the bacterial suspension was dropped onto the surface of the meltblown fabric and graphene-meltblown fabric, which were obtained from the C-mask and P-mask, respectively. After being treated with solar irradiation (200% of full-sun intensity, 5 min), the bacterial solution was collected and diluted from 10^1 to 10^5 with a dilution factor of 10 in sterile PBS. 20 μL of the diluted bacterial solution was cultured on an LB agar plate at 37°C for 24 h. All experiments were operated on a sterilization table and carried out in quadruplicate. The Xenon lamp was sterilized and placed on a sterilization table during the photothermal experiment. Three diluted bacterial solutions allow viability assessment (CFU counting).

The residual bacterial solution was analyzed by live/dead assay. Before the experiment, 1.5 μL of SYTO 9 and 1.5 μL of propidium iodide were mixed with 1000 μL of PBS and stored in the dark. The bacteria solution was collected from the masks after treatment with or without light irradiation and stained with 100 μL of the staining solution. After incubating in the dark at room temperature for 15 min, the bacteria solution was centrifuged and dispersed with PBS. At last, the cell was imaged by laser scanning confocal microscopy.

The controls without light irradiation for both masks were kept in the dark until the start of the assays. The observations of bacteria were carried out the same as those of the sample treated by light irradiation.

The direct outdoor solar irradiation is carried out on 10 May, 2021 at 22°20′59.2"N 113°35′13.0"E (25°C–29°C, sunny days)

Photothermal reusability of masks

The P-masks were first exposed to steam at 100°C for 30 min. After drying, the P-mask was folded and tightened on a plastic pipe, which was ventilated with N_2 flow (0.04 MPa with a pipe diameter of 7 mm) to simulate human exhalation for 60 min. After that, the P-mask was folded 200 times by hand to test the adhesivity of the functional layer on the meltblown fabric. Before test, it was irradiated for 1 h. The FT-IR and photothermal antibacterial ability of the treated P-mask was tested in the same way as presented above.

Quantification and statistical analysis

The statistics of colony-forming units were carried out as described above and performed in triplicate. ZEN 2.3 software (Carl Zeiss) was used to analyze the Laser scanning confocal microscopy images.